High-temperature reflective sensor based on single fusion-splicing fiber taper without coating

Yingyu Yu (于鹰宇), Lan Jiang (姜 澜), Benye Li (李本业), Sumei Wang (王素梅)*, and Hongbin Wu (吴鸿宾)

NanoManufacturing Fundamental Research Joint Laboratory of National Science Foundation of China, School of Mechanical Engineering, Beijing Institute of Technology, Beijing 100081, China

**Corresponding author: wangsumei@bit.edu.cn*

Received April 13, 2012; accepted August 8, 2012; posted online October 16, 2012

A high temperature sensor based on an ultra-abrupt tapered fiber Michelson interferometer fabricated by the fusion-splicing method is proposed. The sensor consists of a single abrupt taper and the cleaved surface is used as the reflection mirror. The thermal characteristic is investigated at 25 to 1 000 °C. The sensitivity of the sensor is observed to vary with the temperature, that is, 25 and 78 pm/°C at 25–300 and 300–1 000 °C, respectively. The Michelson interferometer sensors have the advantages of simple structure, cost effectiveness, compactness, and simple fabrication process.

OCIS codes: 280.4788, 060.2370, 120.3180.
doi: 10.3788/COL201210.122801.

Optical fiber sensors have attracted increasing research attention for their wide range of applications, including monitoring temperature[1], refractive index (RI)[2], pressure[3], strain[4], and bending[5]. The measurement of temperature based on fiber devices has been studied using various techniques. Such devices include fiber gratings[6], core-cladding-mode interferometers[7,8], and other interesting structures[9]. However, fiber grating-based sensors require complicated fabrication processes. Core-cladding-mode interferometers can be constructed in various ways, such as by linear long-period fiber grating (LPFG) pair[10], abrupt taper pair[11], core-offset attenuator pair[12], combined abrupt fiber taper or core-offset attenuator with LPFG[13,14], and thin-core fiber modal interferometers[15,16]. The thin-core fiber modal interferometers require special fibers, while the fabrication of abrupt taper or core-offset attenuator based interferometers is simple and cost-effective.

A fiber temperature sensor based on the interference of selective higher-order modes, but with sensitivity (15 pm/°C) in circular optical fibers was demonstrated[17]. Dong *et al.*[18] proposed a high-temperature fiber sensor with high sensitivity (68.6 pm/°C) based on a bare small-core-diameter dispersion compensation fiber, but the method required special fibers. Two electric-arc techniques were proposed to make fiber tapers[4,19]. One technique creates a taper by stretching the fiber through the heat of electrical arc discharge[4]. The other technique creates a taper by fusion splicing[19]. Both methods couple light from cores into claddings.

This letter proposes a high temperature sensor based on core-cladding-mode Michelson interferometer. The sensor consists of a single abrupt taper and a cleaved surface. The cleaved surface without coating is used as the reflection mirror. The interferometer is applied for high-temperature sensing. The sensitivities are 25 and 78 pm/°C in the temperature regions of 25–300 and 300–1 000 °C, respectively.

The schematic diagram of the proposed Michelson interferometer is shown in Fig. 1(a). The fiber inline Michelson interferometer is fabricated by a conventional fusion splicer (IFS-9, INNO INSTRUMENT Inc., Korea). Two cleaved fiber ends are separated by a certain distance through the programmed fusion splicer. The two normal cleaved ends become ellipsoidal by a one-time discharge. The two ellipsoidal heads are moved to be contacted in the center of the splicer electrodes and fused together by another discharge. The free end of the fiber taper is cleave-separated by a distance of L. Proper discharge arc duration and the current of the electrodes minimize the losses and achieve robust splices.

A detection system consisting of a tunable laser (Agilent 81980A) and an optical power meter (Agilent 8163B) measures the reflection spectra by wavelength sweeping. The measurement system is shown in Fig. 1(b). The tunable laser scans through its wavelength range (1 465 to 1 575 nm) at a rate of 5 pm/step. The signal reflected from the device at each wavelength step is recorded by an optical power meter. Controlling the fusion-splicing condition, such as the discharge current and duration, obtains strong interference signals, even with short interferometer lengths. The reflection spectra of the sensors with different lengths are shown in Fig. 2. The extinction ratios (attenuation difference of maximum and minimum values) are 13, 16, and 7 dB for interferometers with lengths of 5, 20, and 40 mm, respectively.

To determine the cladding modes that construct the interference, the fast Fourier transform (FFT) of the wavelength spectra is performed to obtain its corresponding spatial frequency spectra, as shown in Fig. 3. The relationship between the spatial frequency and the interferometer length as well as the differential modal group index is given by[20]

$$\xi = \frac{2}{\lambda_0^2} \Delta m_{\text{eff}} L, \tag{1}$$

where λ_0 is the center wavelength, ξ is the spatial frequency, and Δm_{eff} is the differential modal group index.

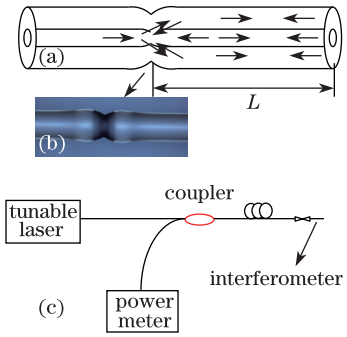

Fig. 1. Proposed Michelson interferometer consisting of one ultra-abrupt fiber taper, (a) schematic diagram of the interferometer, (b) microscopic image of the fabricated taper, and (c) schematic diagram of the spectra measurement system.

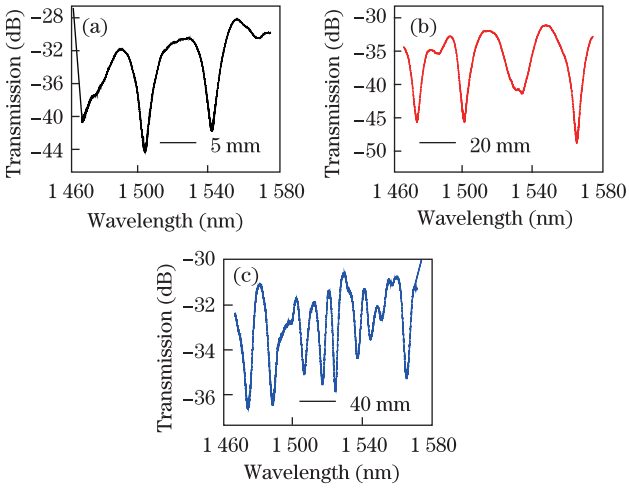

Fig. 2. Reflection spectra of interferometers fabricated by electric-arc discharge with various L, (a) 5, (b) 20, and (c) 40 mm.

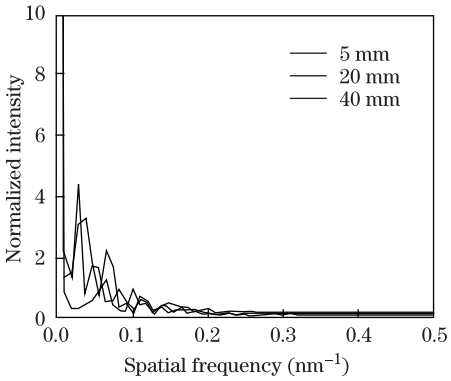

Fig. 3. (Color online) Spatial frequency spectra by taking the FFT for the three interferometers.

For a fixed length, a smaller ξ corresponds to a smaller Δm_{eff}, which means a lower-order cladding mode. For a fixed Δm_{eff} (a fixed cladding mode), ξ decreases as the interferometer length L decreases[18]. Figure 3 shows that the peak amplitudes are located at $\xi = 0.027$, 0.036, and 0.064 nm^{-1} for the interferometers with lengths of 5, 20, and 40 mm, respectively.

Numerous cladding modes with different effective RIs can be excited when light is transmitted through the ultra-abrupt fiber taper. The cleaved fiber surface end functions as a mirror, and the cladding modes are reflected and coupled into counterpropagating cladding modes before being coupled back into the core at the taper section[21]. The interference signal reaches its minimum when the phase difference between cladding and core modes satisfies the following condition[7]:

$$4\pi \left(n_i^{\text{eff}} - n_j^{\text{eff}}\right) \frac{L}{\lambda_v} = (2k+1)\,\pi, \tag{2}$$

where L is the interferometer length, k is an integer, λ_v is the maximum attenuation wavelength of the kth order, and n_i^{eff} and n_j^{eff} are the effective RIs of two interference modes, respectively. The interference pattern of the interferometer is determined by all the modes that match the aforementioned interference condition. Thus, nonhomogeneous spectra are seen in Fig. 2.

Although more than two modes participate in the interference, the energy is mainly distributed in the fundamental mode and in one or two cladding modes. Thus, two main modes are sufficient to qualitatively analyze the performance of the interferometer to the external temperature. With changes in ambient temperature, the mode index difference Δn_{eff} and the fiber length L change accordingly. The response of the Michelson interferometer sensor to the temperature change can be deduced as

$$\frac{\mathrm{d}\lambda_v}{\mathrm{d}T} \cong \left[\frac{4L}{2k+1}\left(\frac{\partial \Delta n_{\text{eff}}}{\partial n_{\text{core}}}\frac{\mathrm{d}n_{\text{core}}}{\mathrm{d}T} + \frac{\partial \Delta n_{\text{eff}}}{\partial n_{\text{cl},j}}\frac{\mathrm{d}n_{\text{cl},j}}{\mathrm{d}T}\right) + \frac{\lambda_v}{L}\frac{\mathrm{d}L}{\mathrm{d}T}\right] \Big/ \left(1 - \frac{4L}{2k+1}\frac{\partial \Delta n_{\text{eff}}}{\partial \lambda}\right), \tag{3}$$

where n_{core} and $n_{\text{cl},j}$ are the effective RIs of the core mode (fundamental mode) and the jth cladding mode, respectively; Δn_{eff} is the effective RI difference between the core mode and the jth cladding mode. When ambient temperature rises, the attenuation peak wavelength redshifts because the thermal-optic coefficient of the Ge-doped silica core is higher than the fused silica cladding thermal-optic coefficient.

The interferometer is placed in a tube furnace (GHA 12/300, Carbolite, Inc.) for the temperature measurements. The end of the interferometer is fixed to keep the Michelson interferometer upright. The interferometer is initially heated to 1 000 °C at the rate of 8 °C/min and maintained at 1 000 °C for 1 h to remove the fiber coating and examine whether the high temperature can seriously deteriorate the reflection spectrum. Figure 4 shows that the attenuation peak shifts to a shorter wavelength for approximately 9.21 nm compared with the original spectrum after the interferometer cools down to room temperature. The blueshift of the spectra may be induced by releasing the mechanical stress caused by the fusion-splicing process.

For the second heating process, the temperature is increased from 25 to 1 000 °C at the rate of 5 °C/min. The spectra of the Michelson interferometer are recorded with an interval of 25 °C. The wavelength shifts of peak A (marked in Fig. 4) with temperature increases is shown

in Fig. 5. The inset shows the measured reflection spectra at different temperatures. Fitting the measured data using a third-order polynomial obtains good cubic expression between the wavelength shift and temperature, with an adjusted correlation coefficient square as high as ∼0.997. Linear fitting in two different temperature ranges estimates the thermal sensitivity to be approximately 25 pm/°C in the low-temperature range (25 to 300 °C) and 78 pm/°C in the high-temperature range (300 to 1 000 °C). Therefore, the interferometer can sense temperature within a certain temperature range; it is especially appropriate for high-temperature sensing because of its high sensitivity. The spectrum of the interferometer is also recorded after the device cools down to room temperature, which is almost identical to the spectrum before the second heating process, as shown in the inset of Fig. 5.

The nonlinearity of the wavelength shift with temperature increases in the whole temperature range (25 to 1 000 °C) may be explained by following: the fusion-splicing region changes the excitation condition with the temperature increases, that is, different sets of cladding modes are excited at different temperatures. As shown in Fig. 6, the FFT of the wavelength spectra of the interferometer at 25 and 800 °C obtains its corresponding

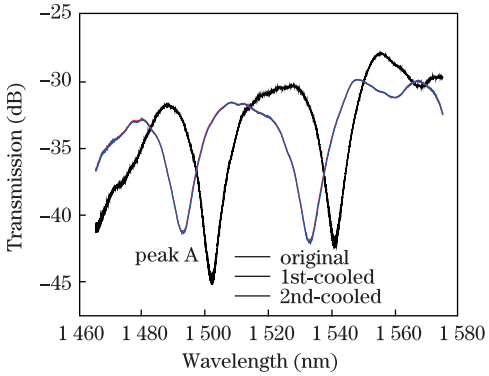

Fig. 4. (Color online) Reflection spectra of Michelson interferometer with length of 5 mm before heating and after heating for the first and second time.

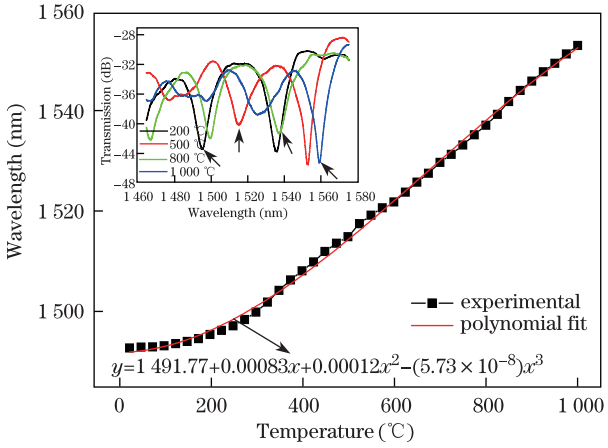

Fig. 5. (Color online) Response of peak A (marked in Fig. 4) of the Michelson interferometer with a length of 5 mm to increases of temperature. Inset is the reflection spectra subject to several temperatures.

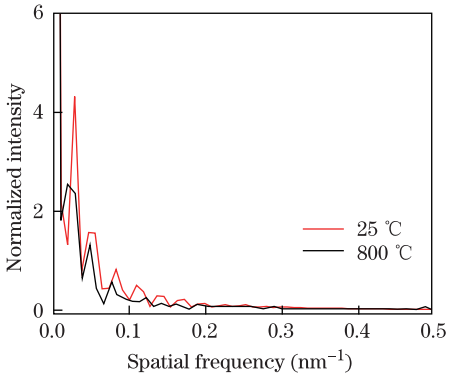

Fig. 6. (Color online) Spatial frequency spectra by taking the FFT for the interferometer with length of 5 mm at 25 and 800 °C.

spatial frequency spectra and determines the cladding modes contributing to the interference. Figure 6 shows that the peak amplitudes of the interferometer are located at ξ = 0.027 and 0.018 nm^{-1} at 25 and 800 °C. It demonstrates that the reflection mode changes with the increase of external temperature, which may cause temperature-sensitivity nonlinearity. In addition, the fiber core and cladding materials are slightly inhomogeneous and the two ellipsoidal head fabricated by one time discharge are not identical. Thus, the bending deflection to the fiber could be induced in the heating process with the release of the residual stress resulting from the fusion splicing process. The bending deflection may be also a minor reason for the nonlinearity.

In conclusion, a high temperature sensor based on core-cladding-mode Michelson interferometer is proposed. The sensor consists of a single abrupt taper and a cleaved surface without using coating as the reflection mirror. The interferometer is applied in high-temperature sensing with 25 and 78 pm/°C sensitivities in the temperature regions of 25–300 and 300–1 000 °C, respectively. The simple fabrication process using the Michelson interferometer presents the possibility of commercial applications in high-temperature measurements.

This work was supported by the National "973" Program of China (No. 2011CB013000) and the National Natural Science Foundation of China (Nos. 90923039 and 51105038).

References

1. L. Jiang, J. Yang, S. Wang, B. Li, and M. Wang, Opt. Lett. **36,** 3753 (2011).
2. L. Jiang, L. Zhao, S. Wang, J. Yang, and H. Xiao, Opt. Express **19,** 17591 (2011).
3. X. M. Zhang, Y. Liu, H. Bae, C. Pang, and M. Yu, Opt. Express **17,** 23965 (2009).
4. Z. Tian and S. S.-H. Yam, IEEE Photon. Technol. Lett. **21,** 161 (2009).
5. O. Frazão, R. Falate, J. L. Fabris, J. L. Santos, L. A. Ferreira, and F. M. Araújo, Opt. Lett. **31,** 2960 (2006).
6. S. W. James and R. P. Tatam, Meas. Sci. Technol. **14,** 49(2003).
7. T. Wei, X. Lan, and H. Xiao, IEEE Photon. Technol. Lett. **21,** 669 (2009).

8. B. B. Gu, M. J. Yin, A. P. Zhang, J. W. Qian, and S. He, Opt. Express **17,** 22296 (2009).
9. Y. Jung, S. Lee, B. H. Lee, and K. Oh, Opt. Lett. **33**, 2934 (2008).
10. T. Allsop, R. Reeves, D. J. Webb, I. Bennion, and R. Neal, Rev. Sci. Instrum. **73,** 1702 (2002).
11. P. Lu, L. Men, K. Sooley, and Q. Chen, Appl. Phys. Lett. **94,** 131110 (2009).
12. Z. Tian, S. S-H. Yam, and H. P. Loock, IEEE Photon. Technol. Lett. **20,** 1387 (2008).
13. X. Dong, L. Su, P. Shum, Y. Chung, and C. C. Chan, Opt. Commun. **258,** 159 (2006).
14. P. Lu and Q. Chen, IEEE Photon. J. **2**, 942 (2010).
15. T.-H. Xia, A. P. Zhang, B. Gu, and J.-J. Zhu, Opt. Commun. **283,** 2136 (2010).
16. J.-J. Zhu, A. P. Zhang, T. H. Xia, S. He, and W. Xue, IEEE Sensors J. **10,** 1415 (2010).
17. E. B. Li, X. L. Wang, and C. Zhang, Appl. Phys. Lett. **89,** 091119 (2006).
18. B. Dong, L. Wei, and D.-P. Zhou, Appl. Opt. **33,** 6466 (2009).
19. B. Li, L. Jiang, S. Wang, L. Zhou, H. Xiao, and H.-L. Tsai, Sensors **11,** 5729 (2011).
20. L. V. Nguyen, D. Hwang, S. Moon, D. S. Moon, and Y. Chung, Opt. Express **16,** 11369 (2008).
21. O. Frazão, P. Caldas, F. M. Araújo, L. A. Ferreira, and J. L. Santos, Opt. Lett. **32,** 1974 (2007).